Selective lithium extraction from diluted binary solutions using metal-organic frameworks (MOF)-based membrane capacitive deionization (MCDI)

Hanwei Yu[1], Sayed Mukit Hossain[1], Chen Wang[1], Youngwoo Choo[1], Gayathri Naidu[1], Dong Suk Han[2] and Ho Kyong Shon[1,*]

[1]ARC Research Hub for Nutrients in a Circular Economy, Center for Technology in Water and Wastewater, School of Civil and Environmental Engineering, Faculty of Engineering and IT, University of Technology Sydney, P.O. Box 123, Broadway, NSW 2007, Australia

[2]Center for Advanced Materials & Department of Chemical Engineering, Qatar University, P.O. Box 2713, Doha, Qatar

Abstract

The increasing demand for lithium (Li) calls for exploring efficient and environmental-friendly methods to extract Li from brine. Capacitive deionization (CDI) as an emerging technology is of interest for resource recovery because of its rapid adsorption rate, limited energy consumption, and low environmental impact. However, Na and K in seawater and seawater reverse osmosis (SWRO) brine and Mg and Ca in inland brine challenge the feasibility of selective Li extraction. Herein, CDI was integrated with deposition-coated ZIF-8-PDA membranes to extract Li from binary solutions containing Li and M (M representing Na, K, Mg, and Ca). MCDI tests were conducted under a series of voltages (±0.5 V, ±1.0 V, and ±1.5 V) to investigate the influence of applied potentials on Li extraction performances. The results indicated advantages for Li extraction when coexisting cations were monovalent than divalent. Additionally, a lower voltage of 0.5 V could provide superior Li selectivity, charge efficiency (CE), and energy normalized to Li (ENL) than higher voltages. Especially, Li selectivity of 1.50 and 1.85 was achieved in Li/Na and Li/K feeds under 0.5 V, 37% and 74% higher than those under 1.5 V, respectively, illuminating the potential of MCDI for Li extraction from seawater and SWRO brine with low energy input.

Keywords: Lithium extraction; Zeolitic imidazolate framework-8; Membrane capacitive deionization; Ion-selective membrane; Mono and divalent cations

1. Introduction

Lithium (Li), one of the key elements applied in electric vehicles and mobile devices, has become highly demanded, prompted by the rapid development of the lithium-ion battery industry [1, 2]. From 2010 to 2021, global Li consumption boomed nearly 4 times, from 24.5 kt to 93.0 kt [3, 4]. Given that over 99.9% of Li is reserved in the ocean and about 75% of Li on land is stored in brine, it is of great value to recover Li from aqueous resources from a business perspective and develop eco-friendly Li extraction materials and processes from an environmental perspective.

Conventional approaches to selectively extracting Li from brine include solvent extraction and adsorption [5, 6]. Whereas solvent extraction can separate Li from brine with a high Mg/Li ratio, the lifespan of the equipment can be limited due to the corruption of organic solvents, and the disposal of solvent leakage can be complicated. Adsorption is widely studied and has been applied in the real-world industry due to the merits of low cost, high Li selectivity, and simple operation process [7], but the processes of adsorbent granulation and ad/desorption are time-consuming. In addition, the acid stripping process for adsorbent regeneration can produce hazardous secondary waste.

To further overcome the drawbacks of conventional approaches and improve Li extraction efficiency, Li separation performances, and environmental friendliness, emerging technologies, for example, electrochemical [8-11] and membrane-based processes [12, 13] have been paid more considerable attention in the past decade. Electrodialysis (ED) can separate monovalent and multivalent ions efficiently combined with nanofiltration (NF) membranes [13, 14] and ion-exchange membranes (IEM) [15, 16]. However, the high energy inputs weaken its economic feasibility. What is more, the separation of Li and other monovalent metal ions is still challenging. In contrast, capacitive deionization (CDI), a novel environmental-friendly technology for facile desalination depending on the electrosorption process [17-19], presents great benefits of technical simplicity, affordable cost, mild operation conditions, and low energy inputs. It takes advantage of low voltages (usually $\leq$ 1.5 V), impelling cations and anions towards the oppositely charged electrodes composed of two porous electrode materials characterized by a high specific surface area. Then the temporarily adsorbed ions are released into the solution by a reverse charge [17]. This technology has attracted increasing attention in this century and is regarded as a promising solution to ion removal, energy harvesting, water purification, and resource recovery as a next-generation technology [20-22].

The research on Li recovery using CDI systems focused on material synthesis, electrode fabrication, cell architecture design, and operation process enhancement. Ion selectivity can be determined by the effect of ion size and valence on the diffusion rate under an electric field [23, 24], and the pore-size distribution of electrode materials can affect salt adsorption capacity and ion selectivity [25, 26]. Nevertheless, the electrode materials are reported as a critical factor influencing CDI performances [24, 27, 28]. Manganese oxide-based electrodes are widely studied because of their extraordinary Li selectivity [27, 29, 30]. Other metal oxide-based electrodes, e.g., Li_3VO_4 and Co_3O_4, also exhibited outstanding adsorption performance [31, 32]. Some research emphasized CDI process enhancement by evaluating various working modes and optimizing operation conditions of feed concentrations and flow rates [33, 34]. In addition, the investigation of novel CDI cell architectures highlights membrane CDI (MCDI), flow-electrode CDI (FCDI), and hybrid CDI (HCDI) [35-38]. Particularly, MCDI, a modification of classical CDI by introducing ion-exchange membranes (IEM) or ion-selective membranes (ISM) between two opposite electrodes, can avoid co-ion repulsion, reduce anode oxidation and energy consumption, increase deionization efficiency and adsorption capacity, and work with low-concentration solutions ($\leq$ 20 mM) [39, 40]. The incorporation of membranes can tune the pore size distribution of an electrode or adjust chemical contacts with target ions, improving ion selectivity.

Currently, metal-organic frameworks (MOFs) have gained great interest in the fabrication of ion-selective membranes. They are organic-inorganic hybrid materials with intermolecular pores formed by self-assembling organic ligands and inorganic metal ions or clusters through coordination bonds [41]. After originally proposed by Yaghi in 1995, MOFs were reported with many subclasses, such as UiOs, Materials of Institute Lavoisier frameworks (MILs), and zeolitic imidazolate frameworks (ZIFs) [42]. ZIF families, built by metal ions, such as zinc (Zn) and cobalt (Co) ions, and nitrogen atom-linked ditopic imidazole anions, have been widely utilized in gas storage and separation, resource recovery, catalysis, sensing, and drug transportation due to their abundant designable structural types, low density, permanent holes, high specific surface area, and functional hole space [43-46]. Especially, ZIF-8 is acknowledged as a promising material for metal recovery applications as it has a homogeneous porosity appearance with substantial surface areas [47]. Zhang et al. confirmed the possibility of three-dimensional ZIF-8 membranes for Li separation. The simulation study revealed that the ionic dehydration-rehydration interactions in sub-nano pore channels could contribute to the difference in ion-transport rates [48]. Based on this mechanism, Mohammad et al.

fabricated a ZIF-8-based composite membrane for Li extraction, which could separate monovalent and divalent ions [49]. However, separating Li from other monovalent cations is still challenging. Hossain et al. prepared AC/ZIF-8 and AC/ZIF-8/CEM cathodes for CDI systems by coating ZIF-8 double layers on activated carbon (AC) electrodes via an in-situ growth method. Their electrosorption results demonstrated successful separations of Li from Na/K coexisting binary solutions [50].

Nevertheless, ZIF-8 was reported to easily hydrolyze into zinc and imidazolate ions within 24 h in aqueous solutions due to the weak bonds of metal nodes and ligands [51]. The poor hydro-stability would limit its long-time applications in water treatment. Thus, many strategies were proposed for ZIF-8 modification to address the water stability problem, such as surface ligand exchange with 5,6-dimethylbenzimidazole (DMBIM) [52, 53] and surface functionalization by incorporating deoxyribonucleic acid (DNA)/polydopamine (PDA) [54, 55]. PDA, a mussel-inspired adhesive cross-linker that can be easily obtained through dopamine (DA) self-polymerization at alkaline aerobic conditions, can tether N and O containing materials by forming covalent and noncovalent bonds [56, 57]. By encapsulating ZIF-8 nanoparticles in PDA, hydrolysis could be inhibited since water molecules would form hydrogen bonds with hydroxyl groups on the surface and difficultly enter the interior of ZIF-8 [58].

Based on the considerations above, we employed PDA as an adhesive to bind ZIF-8 crystals strongly. The composite ZIF-8-PDA membrane was doubly coated on commercial AC electrodes via a deposition coating method. The fabricated AC/ZIF-8-PDA electrodes were assembled into a batch MCDI setup as cathodes while anion exchange membrane (AEM)-coated electrodes were used as the counter ones. This study investigated the Li extraction performances of the MCDI system using diluted binary brines (containing Li and M; M representing Na, K, Mg, and Ca) as feeds. In addition, the MCDI tests were conducted with voltages of ±0.5 V, ±1.0 V, and ±1.5 V to study the influence of applied voltages on Li selectivity, Li adsorption capacity (LAC), charge efficiency (CE), and energy normalized to Li (ENL). Overall, this work broadened the use of ZIF-8 for AC electrode modification and validated the MCDI technology as a promising method for Li recovery from diluted brine.

2. Materials and methods

2.1 Materials

The materials for ZIF-8-PDA synthesis included zinc nitrate hexahydrate ($N_2O_6Zn_6 \cdot H_2O$, molar mass: 297.49 g/mol), solvent 2-Methylimidazole (2-mIM) ($C_4H_6N_2$, molar mass: 82.10 g/mol,), methanol (CH_3OH, molar mass: 32.04 g/mol, suitable for HPLC), Tris(hydroxymethyl)aminomethane (Tris) ($NH_2C(CH_2OH)_3$, molar mass: 121.14 g/mol), and dopamine hydrochloride ($(HO)_2C_6H_3CH_2CH_2NH_2 \cdot HCl$, molar mass: 189.64 g/mol) were provided by Sigma Aldrich.

The binary feed solutions were prepared using lithium chloride (LiCl, molar mass: 42.39 g/mol, reagent grade), sodium chloride (NaCl, molar mass: 58.44 g/mol), potassium chloride (KCl, molar mass: 74.55 g/mol), anhydrous magnesium chloride ($MgCl_2$, molar mass: 95.21 g/mol), and anhydrous calcium chloride ($CaCl_2$, molar mass: 110.98 g/mol) obtained from Sigma Aldrich.

For the assembly of the MCDI setup, the acryl unit cell, AC electrodes, and AEM-coated AC electrodes were collected from Siontech Co., Ltd. Whatman glass fiber prefilters with 2-μm pores were employed in MCDI cells as the spacers. Milli-Q (MQ) water was utilized to produce feed solutions. All compounds in the experiments were utilized as supplied without additional purification.

2.2 Preparation of AC/ZIF-8-PDA electrodes

The schematic illustration of the electrode preparation process is depicted in **Fig. 1**. ZIF-8 crystals were synthesized in methanol at room temperature for 72 h, according to a number of published papers [59, 60]. The precursor solution for ZIF-8 growth was prepared by mixing 1.2 g of $Zn(NO_3)_2 \cdot 6H_2O$ and 26.62 g of 2-Methylimidazole in 150 mL of methanol in a beaker under magnetic stirring for 72 h. The pH of the ZIF-8 seeding solution was adjusted to alkaline (around 9) with Tris. For ZIF-8-PDA synthesis, 0.6 g of dopamine hydrochloride was dissolved in 50 mL methanol, then mixed with ZIF-8 seeding solution followed by stirring for 12 h. Before electrode modification, ZIF-8-PDA was washed three times using methanol to remove superfluous 2-mIM and PDA and was stored in methanol. Then, the deposition coating method was adopted twice under room temperature for electrode coating, transferring 30 mL of the ZIF-8-PDA seeding solution mentioned above per time on the AC electrode fixed by a square

acrylic mold of 100 cm^2 internal area and waiting until the solvent was fully evaporated. Subsequently, the electrode was rinsed thrice with methanol and MQ water, respectively, and dried at room temperature. The fabricated electrodes were preserved in a desiccator before use.

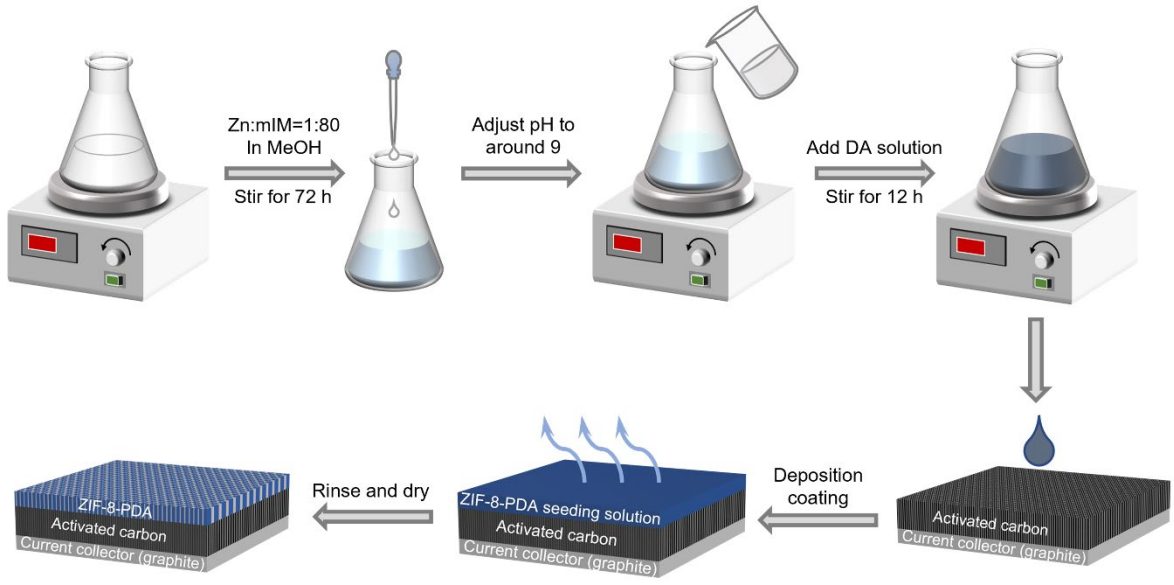

Figure 1. Schematic illustration of ZIF-8-PDA synthesis and AC/ZIF-8-PDA electrode fabrication.

2.3 Characterization

The morphologies of ZIF-8-PDA particles, bare AC electrode surface, and the membrane surface along with the cross-section of AC/ZIF-8-PDA electrode were characterized by scanning electron microscopy (SEM, Zeiss Supra 55VP). The elemental compositions of the ZIF-8-PDA layer were measured using an energy-dispersive X-ray spectroscopy detector (EDS, Oxford). The chemical composition and functional groups of the ZIF-8 and ZIF-8-PDA particles were recognized using Fourier transform infrared (FT-IR) spectroscopy (IRPrestige-21) in the wavenumber range of 400 – 4000 cm^{-1}. The crystalline phases of ZIF-8 particles were identified by X-ray powder diffractometer (XRD, Bruker D8 Discover) with Cu Kα radiation source at a scanning rate of 0.04°/s from 0.5° to 50°. The nitrogen isotherm measurement was performed with a Quantachrome Analyzer (Micromeritics TriStar II Plus, Australia). The ZIF-8-PDA particle sample was degassed for 10 h at 150 °C. The Brunauer–Emmett–Teller (BET) method was used to determine the specific surface area of ZIF-8-PDA particles. The pore size distribution was analyzed based on the non-local density functional theory (DFT), and the total volume was measured at a relative pressure (P/P_0) over 0.99.

2.4 Static water stability verification of ZIF-8-PDA

The water stability test was conducted by immersing ZIF-8-PDA particles in water and observing the transformations of morphology and crystalline phase, following the published studies towards MOF water stability [61, 62]. It was reported that the hydrolysis of ZIF-8 can be reflected in the morphology shift from diamond dodecahedron to leaf shape [63]. The ZIF-8-PDA particles were added into Milli-Q water at predetermined ratios of 2 wt%, 5 wt%, 10 wt%, and 20 wt% and soaked for 24h. Later, the particles were collected by centrifuging at a rate of 4000 rpm/min for 10 mins, removing water, and drying in an oven at 60°C overnight. The morphologies of the obtained water-soaked particles were monitored by SEM. In addition, XRD patterns of the ZIF-8-PDA particles fully soaked in water for one month and the ZIF-8 soaked for one day were measured and compared with pristine ZIF-8-PDA peaks.

2.5 MCDI setup

A diagram of the lab-scale MCDI module and cell is presented in **Fig. 2**. The MCDI system (**Fig. 2a**) consisted of a potentiostat for providing constant charge potentials, a computer for recording and analyzing the data of current, voltage, power, and resistance, a multimeter for monitoring pH and conductivity, an MCDI cell for electrosorption, a reservoir containing binary feed solution, and a peristaltic pump for circulating the solution flow in the system. The multimeter measured and recorded the real-time data every 10 seconds. The peristaltic pump was set to a constant flow rate (20 mL/min). 1 mL of effluent samples were collected from the solution reservoir every 2 or 5 mins for cation composition analysis. The potentiostat (Autolab PGSTAT302N, Metrohm) delivered charging potentials of -0.5 V, -1.0 V, and -1.5 V in the electro-adsorption process for Li extraction and discharge potentials of 0.5 V, 1.0 V, and 1.5 V in the electro-desorption processes for ion recovery and electrode regeneration. The binary feed solutions contain 10 mM LiCl and MCl_x (M = associated coexisting cations (Na, K, Mg, or Ca), x = 1 or 2). As **Fig. 2b** shows, the assembly of the MCDI cell comprised an AC/ZIF-8-PDA electrode, an AC/AEM (thickness of 170 μm) electrode, and a glass fiber spacer (Whatman, thickness of 250 μm). The solution flowed in the assembly from the edge, then down the spacer channel, and finally out via the central outlet. 20-min cycles were repeated trice for the electrosorption/desorption tests with each type of feed solution.

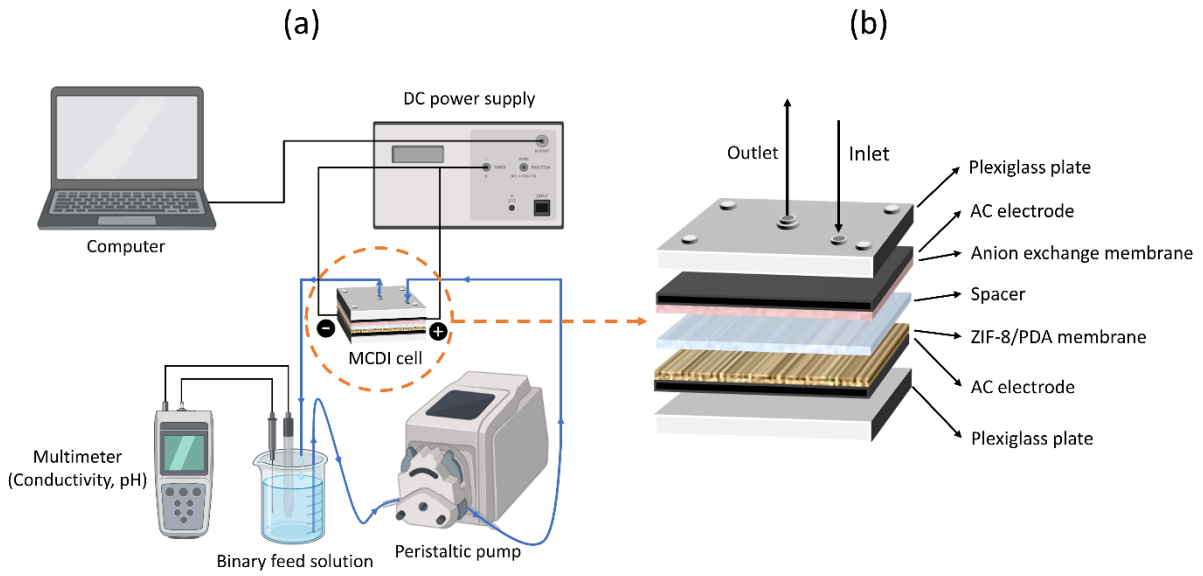

Figure 2. Schematic illustration of the experimental design.

2.6 Li extraction test under different voltages

Li extraction performances were tested using the MCDI system with constant hydraulic residence times and a series of equimolar binary feed solutions containing Li and M (M representing the associated coexisting cations). To compare the competing ion removal in the electrosorption process, four mono and divalent alkali and alkali earth metals with similar ionic sizes to Li were selected as coexisting cations, i.e., Na, K, Mg, and Ca. Na and K are abundant in seawater and seawater reverse osmosis (SWRO) brine, and Mg and Ca are core competitors in Salt Lake brine. The MCDI tests using Li/Na and Li/K binary feed are named monovalent cases, and those using Li/Mg and Li/Ca binary feed are appointed divalent cases. The bare and hydrated ionic radii and their hydration enthalpy are listed in **Fig. 3**. Typically, these cations exist in hydrated forms in aqueous solutions with the order of hydrated ionic radii being Mg (4.28Å) > Ca (4.12Å) > Li (3.82Å) > Na (3.58Å) > K (3.31Å). However, in their bare states, the order is K (1.33Å) > Ca (0.99Å) > Na (0.95Å) > Mg (0.65Å) > Li (0.60Å), which suggests the potential to selectively extract Li from other ions based on size effects. The differences in hydration enthalpy values reflect the ease of dehydration for each type of ion, indicating that the variation in energy input into the MCDI system may influence the dehydration processes. To investigate the potential of MCDI for Li extraction from diluted brine resources, an initial concentration of 10 mM for each component and a volume of 200 mL were fixed for all feed solutions.

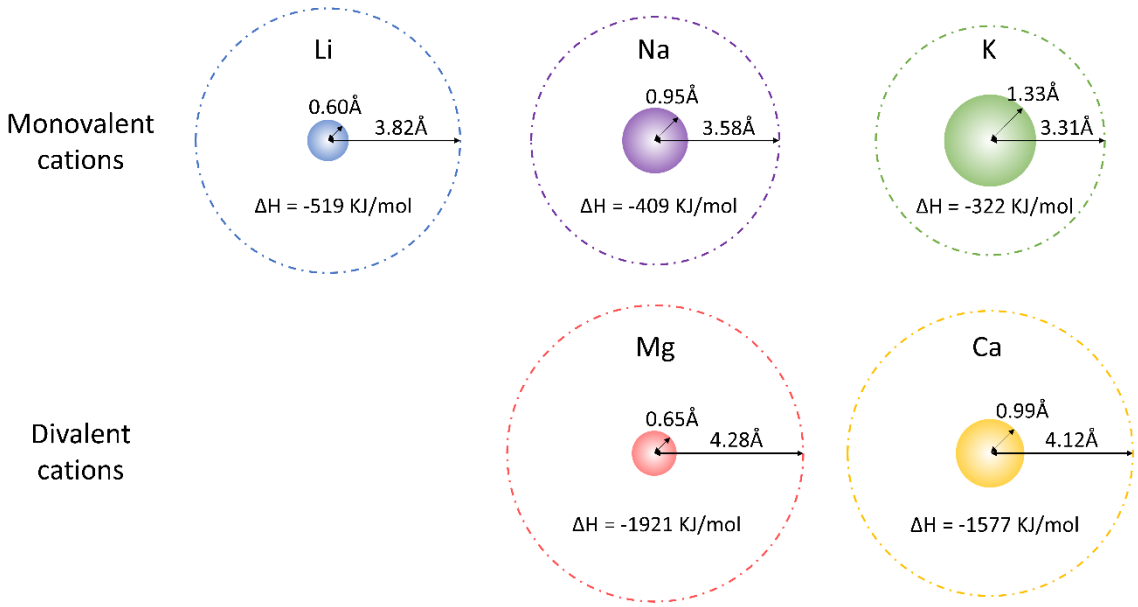

Figure 3. The bare and hydrated ionic radius of Li, Na, K, Mg, and Ca and their hydration enthalpy [64, 65].

The electrosorption processes were firstly carried out at a voltage of -1.0 V, and the subsequent desorptions were at 1.0 V. The duration of adsorption and desorption was both set to 20 min. The effluent samples of 1 mL were collected every 2 mins during the electrosorption phase. To investigate the influence of applied voltages on Li adsorption performance, the MCDI experiments were conducted under ±0.5V and ±1.5V. The concentrations of cations in the samples were measured by inductively coupled plasma mass spectrometry (ICP-MS, Agilent 7900, Agilent Technologies Inc.). The real-time conductivity and pH of the solutions were monitored every 10 seconds. The tests were repeated three times, and the standard average was calculated. Li extraction performances were evaluated in terms of ion removal rate, Li selectivity, LAC, CE, and ENL.

The ion removal rate was calculated with Eq. (1).

$$\eta_x(\%) = (1 - \frac{C_t}{C_0}) \times 100 \qquad (1)$$

Where x is Li, Na, K, Mg, or Ca; η_x is the ion removal rate of x; C_0 is the initial concentration of x; C_t is the concentration of x at time t.

The Li selectivity was calculated with Eq. (2).

$$\rho_M^{Li} = \frac{\eta_{Li}}{\eta_M} \qquad (2)$$

Where M represents the competing cation (Na, K, Mg, or Ca) and ρ_M^{Li} is the relative Li selectivity to M.

Li adsorption weight (LAW) is described as Li removal weight per 100 cm^2 of the cathode, given by Eq. (3), and LAC is defined as the final LAW at the end of each adsorption experiment, i.e., the weight of adsorbed Li per 100 cm^2 of the cathode.

$$\mathrm{LAW_t\ (mg)} = (\mathrm{C_0} - \mathrm{C_t})\mathrm{V} \quad (3)$$

Where V is the feed solution volume.

The CE (Λ) and ENL were calculated by Eq. (4) and (5), respectively.

$$\Lambda\ (\%) = \frac{(C_t - C_0)VF}{M_{Li}\mathrm{Q}} \times 100 \quad (4)$$

$$\mathrm{ENL\ (\mu mol\ J^{-1})} = \frac{(\mathrm{C_t} - \mathrm{C_0})\mathrm{V}}{\mathrm{M_{Li}E_{ad}}} = \frac{(\mathrm{C_t} - \mathrm{C_0})\int \mathrm{I\,dt}}{\mathrm{M_{Li}}} \quad (5)$$

Where F is the Faraday constant (96485 C mol^{-1}); M_{Li} is the molar mass of Li (6.94 g mol^{-1}); Q is the charge supplied per adsorption cycle (C); E_{ad} is the energy supplied during an adsorption cycle during constant voltage MCDI.

3. Results and discussion

3.1 Characterizations of ZIF-8-PDA particles and the modified electrode

Fig. 4 shows SEM images of ZIF-8 particles, the bare AC electrode, and the surface and cross-section of the AC/ZIF-8-PDA electrode. Ultrasmall ZIF-8-PDA particles with the shape of diamond dodecahedrons were synthesized. The bare AC electrode showed an uneven and porous surface composed of AC lumps with varied sizes, which corresponds with published work [66]. The thickness of the carbon layer on the graphite foil was estimated to be 100 μm. After deposition coating, a dense ZIF-8-PDA layer of around 1 μm thick on average fully covered the top of the AC electrode.

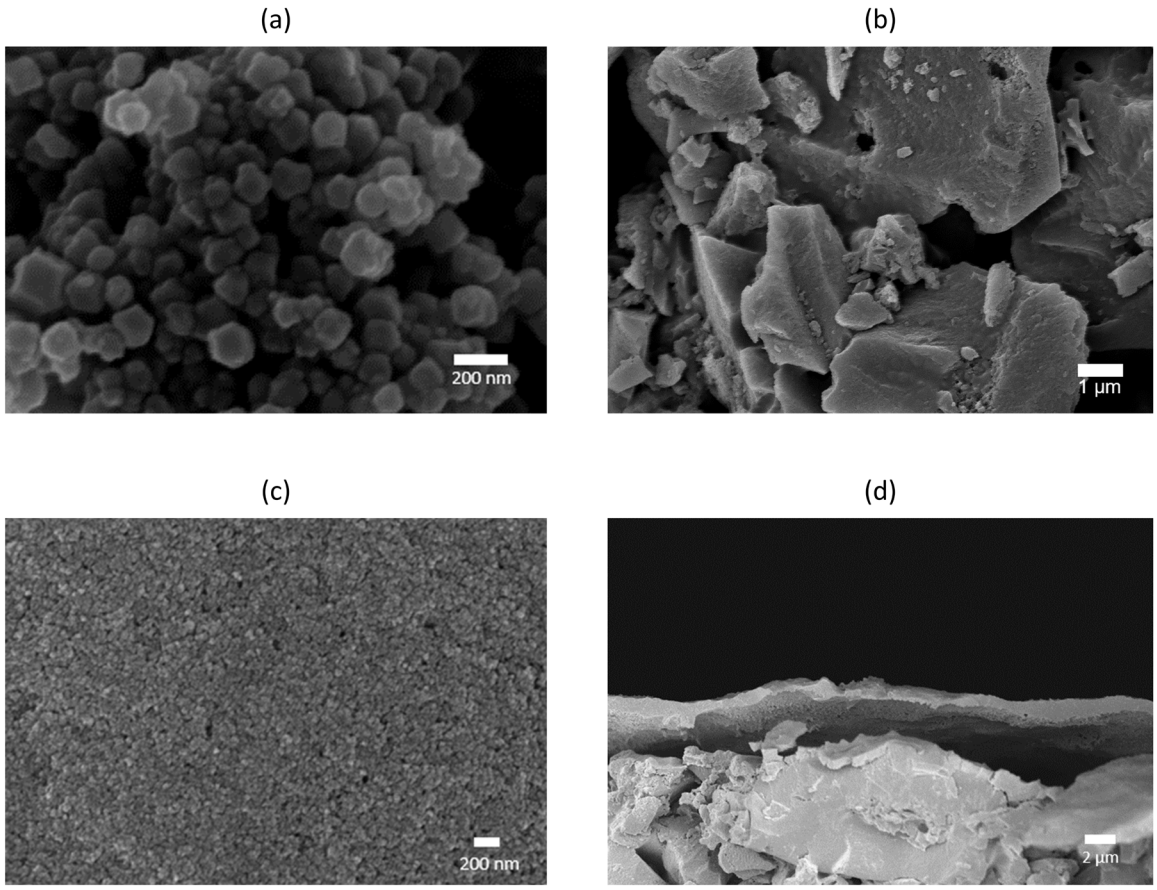

Figure 4. SEM images of (a) ZIF-8-PDA particles, (b) bare AC electrode, (c) the surface of the AC/ZIF-8-PDA electrode, and (d) the cross-section of the AC/ZIF-8-PDA electrode.

The information on the functional groups, element components, micropores, and crystalline phases of ZIF-8-PDA were illustrated in **Fig. 5** and **Fig. 7(c)**, given by FTIR, EDS, BET, and XRD characterizations. The EDS results confirmed the composition of carbon (59.92%), nitrogen (12.07%), oxygen (5.98%), and zinc (22.02%) in ZIF-8-PDA. In the FTIR spectra of ZIF-8 and ZIF-8-PDA, the peaks at 690 and 758 cm^{-1} were associated with Zn-N and Zn-O bonds, respectively; peaks between 990 and 1500 cm^{-1} could be accredited to in-plane and out-of-plane C-N stretching vibration in imidazole groups, and the peaks at 1580 cm^{-1} were related to C=N bonds [67-69]. The type-I nitrogen adsorption isotherm for ZIF-8-PDA showed a dynamic increase in adsorbed N_2 at low relative pressure, indicating the presence of intrinsic micropores. The effective BET surface area of ZIF-8-PDA was estimated to be 175.87 m^2/g, and the pore volume was evaluated as 0.12 cm^3/g. The half pore width of ZIF-8-PDA was calculated to be within 10Å, which could be the main contributor to ion separation. The incorporation of PDA altered the pore size distribution. Compared to ZIF-8, of which the surface area could be larger than 1000 m^2/g [46], ZIF-8-PDA showed low porosity yet wider

pore widths, which could weaken Li sieving performance. The XRD peaks of ZIF-8-PDA particles were identified at the 2-theta positions of 7.39° (110), 10.40° (200), 12.75° (211), 14.75° (220), 16.50° (310), 18.06° (222), corresponding to characteristic peaks of ZIF-8 in literature [53, 55, 58, 60], implying that the crystal structure of ZIF-8 remained intact with the incorporation of PDA.

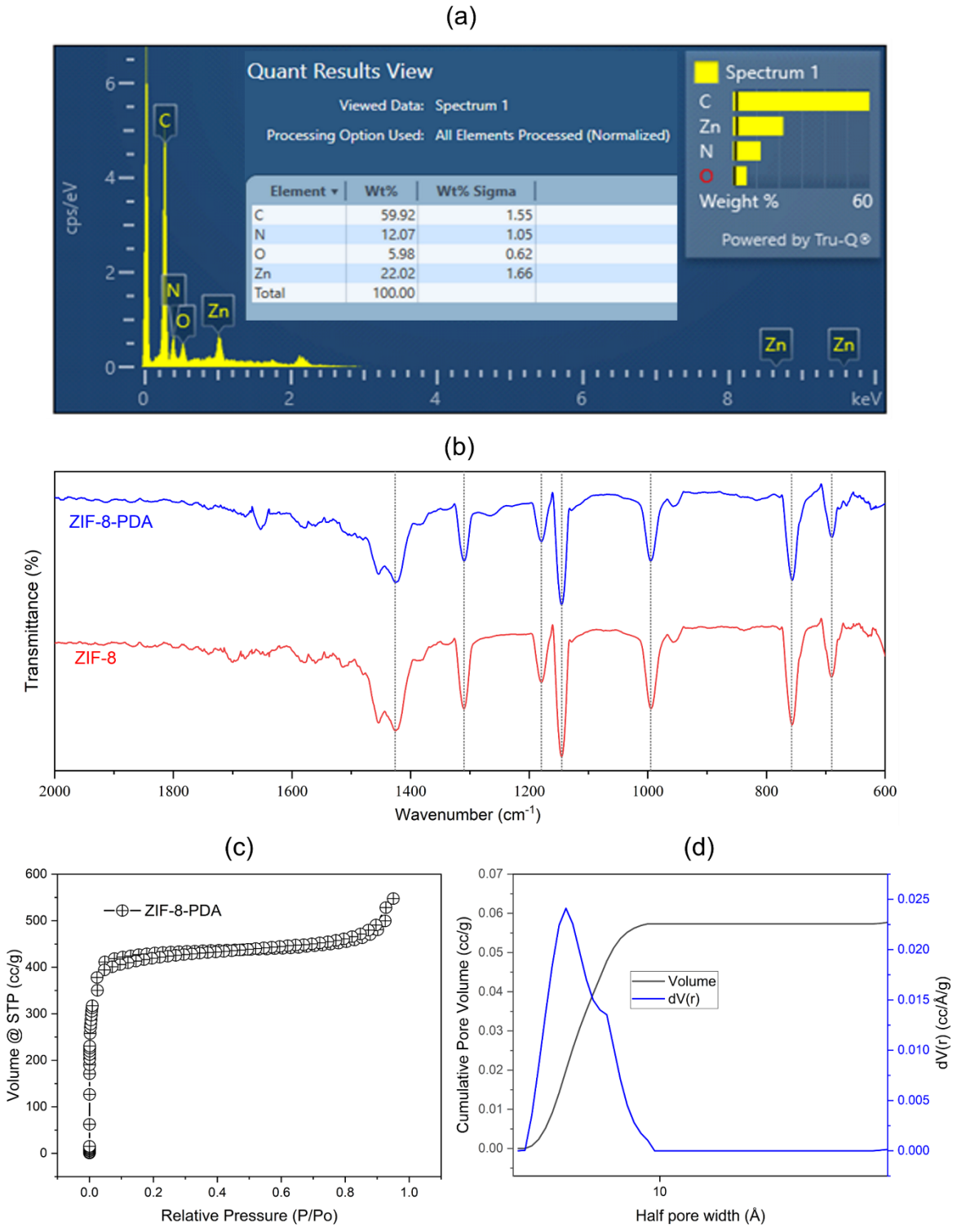

Figure 5. (a) EDS, (b) FTIR patterns, (c) BET analysis, and (d) pore size of the ZIF-8-PDA.

3.2 Water stability of the ZIF-8-PDA particles

Fig. S1 shows the morphologies of the ZIF-8-PDA particles after being immersed in water for 24 h. It can be observed that although some particles changed to smaller spherical and irregular forms, most of the particles kept the original morphology. The degradation proportion slightly increased with the decrease in MOF/water ratio. **Fig. 6** demonstrates SEM images and XRD patterns of the ZIF-8 and ZIF-8-PDA particles after soaking in MQ water for 24 h and one month, respectively. The hydrolyzed ZIF-8 presented leaf- and needle-like shapes, corresponding to other research on ZIF-8 hydrostability [53, 63]. In comparison, the morphology transformation degree of ZIF-8-PDA was much slighter. For XRD results (**Fig.6c**), the crystallinity of the (110) phase reduced significantly, those of the (310) and (222) phases increased, and some unknown peaks appeared with the hydrolysis. Notably, the (100) phase of ZIF-8 almost disappeared, and the positions of many peaks shifted. SEM and XRD results suggested a better water stability of ZIF-8-PDA than ZIF-8, which can be attributed to the protection of PDA. The hydrolysis occurs when ZIF-8 contacts with water molecules, but the presence of PDA could provide a relatively restrained environment to the inner ZIF-8 particles, inhibiting escaping of the hydrolyzed Zn^{2+} and 2-mIM and favoring the re-formation of ZIF-8. The concentrations of Zn^{2+} and 2-mIM could be much higher in the PDA-restrained zone than in water, in which a dynamic equilibrium between ZIF-8 formation and hydrolysis might exist.

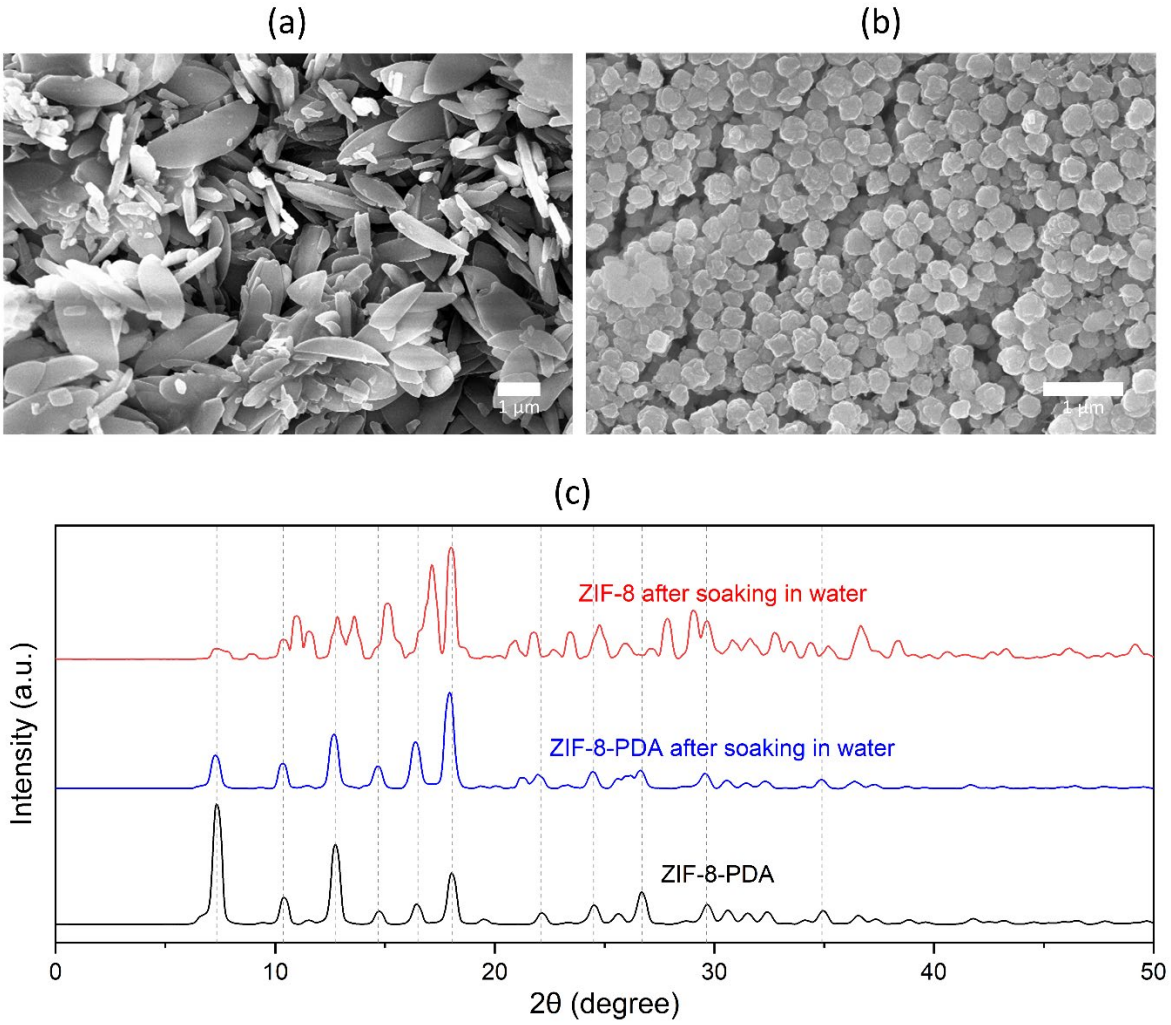

Figure 6. SEM images of (a) hydrolyzed ZIF-8 particles after soaking in MQ water for 24 h and (b) ZIF-8-PDA particles after soaking in MQ water for one month, and (c) XRD patterns of the above ZIF-8 and ZIF-8-PDA after soaking in water.

3.3 MCDI performance under different voltage conditions

3.3.1 MCDI performance under 1.0 V

In our previous study on the CDI performance of bare AC electrodes, binary feed solutions and a CV of 1.0 V were applied in the CDI tests [50]. Similarly, the same feed solution components and charge potential conditions were employed to investigate the MCDI performance incorporating ZIF-8-PDA. The ion removal performance is illustrated in **Fig. S2.** The concentrations of all cations decreased, and the ion removal rates increased with the electrosorption duration, then both remained at a certain level, indicating the saturation of ion adsorption. Finally, the removal rates of all competing ions, i.e., Na, K, Mg, and Ca, were at a similar level, reaching 22.20%, 18.89%, 21.16%, and 20.27%, respectively. However, the Li

removal rate varied in monovalent and divalent cases. The η_{Li} reached 21.11% and 18.37% in Na and K competing cases, respectively, yet were 6.08% and 8.39% when Mg and Ca coexisted. **Fig. S3** presents the conductivity and pH of the solutions during the adsorption and desorption processes. The conductivity in the solutions lowered gradually with the reduction of metal ions and then kept steady, implying the completion of adsorption. Conversely, in the desorption period, the conductivity rose rapidly in the beginning 5 mins with the release of ions and then remained steady at 450-550 μS/cm. The pH raised and reduced slightly in the adsorption and desorption stages, respectively, which could be explained by the electrosorption and release of protons. The metrics of Li selectivity, CE, LAW, and ENL for the ZIF-8-PDA coated AC electrodes are displayed in **Fig. 7**. LAW rose till it reached a saturated level defined as LAC. LAC was over double in monovalent cases than in divalent cases. Li selectivity (ρ_M^{Li}) can reflect the ability to separate Li from binary solutions. Here, ρ_{Na}^{Li}, ρ_K^{Li}, ρ_{Mg}^{Li}, and ρ_{Ca}^{Li} were estimated to be 0.95, 0.97, 0.28, and 0.41, respectively.

Compared to the bare AC electrodes [50], the Li removal rates augmented by 12.3% and 74.5% in Na and K coexisting feeds and decreased by 74.8% and 54.6% in Mg and Ca coexisting feeds, respectively; Li selectivity to Na and K improved by 30.1% and 125.6%, and those to Mg and Ca declined by 58.2% and 29.3%, respectively (see **Fig. 8**). The presence of ZIF-8-PDA built up the preference of electrodes to Li in monovalent cases. Hou and Huang reported that monovalent cations with lower dehydration enthalpy were favorable to be electrosorbed in an AC electrode-based CDI system [70]. However, the size-sieving role of the ZIF-8-PDA layer can promote the monovalent cations with smaller dehydrated ion radius to pass through the membrane. In monovalent and divalent cation mix situations, cations with higher valences are more sensitive in an electric field due to stronger electrostatic attractions. The ZIF-8-PDA membrane as a barrier layer magnified the influence of charge potentials on valences, further facilitating divalent ions to permeate the membrane in priority. However, compared to AC/ZIF-8 electrodes [50], although the water stability improved with the presence of PDA, Li selectivity generally dropped, mainly caused by the increase in pore sizes. Thus, the trade-off between Li selectivity and water stability should be noticed.

CE and ENL were calculated according to the measured current, power, resistance, and electrical charge (shown in **Fig. S4**). These parameters give insight into charge and energy consumption on Li adsorption from the mixed feed stream of the MCDI system. Charges used for achieving Li extraction are considered effective usage, while those consumed by competing ions and electrodes are regarded as charge loss. ENL reflects on the moles of captured Li per

joule energy input. The CE and ENL were computed to be 44.4% and 4.60 μmol/J in Li/Na binary feed, 38.8% and 4.03 μmol/J in Li/K binary feed, 18.7% and 1.94 μmol/J in Li/Mg binary feed, and 18.4% and 1.91 μmol/J in Li/Ca binary feed, respectively. Consistent with LAC and Li selectivity, CE and ENL were markedly higher in monovalent than divalent cases, implying that more Li were extracted per unit of energy input to the monovalent feed MCDI system.

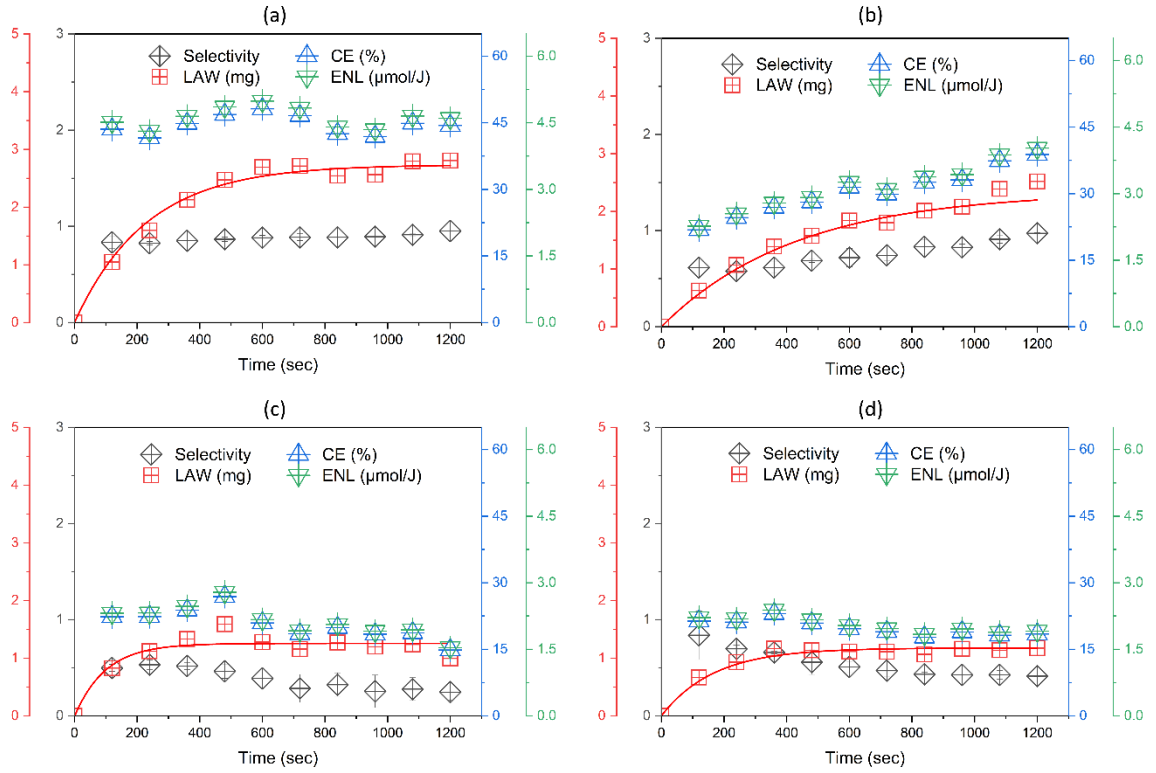

Figure 7. Temporal Li extraction performances of Li selectivity, LAW, CE, and ENL of ZIF-8-PDA coated CDI under 1.0 V by using binary feed solution of (a) Li/Na, (b) Li/K, (c) Li/Mg, and (d) Li/Ca mixes.

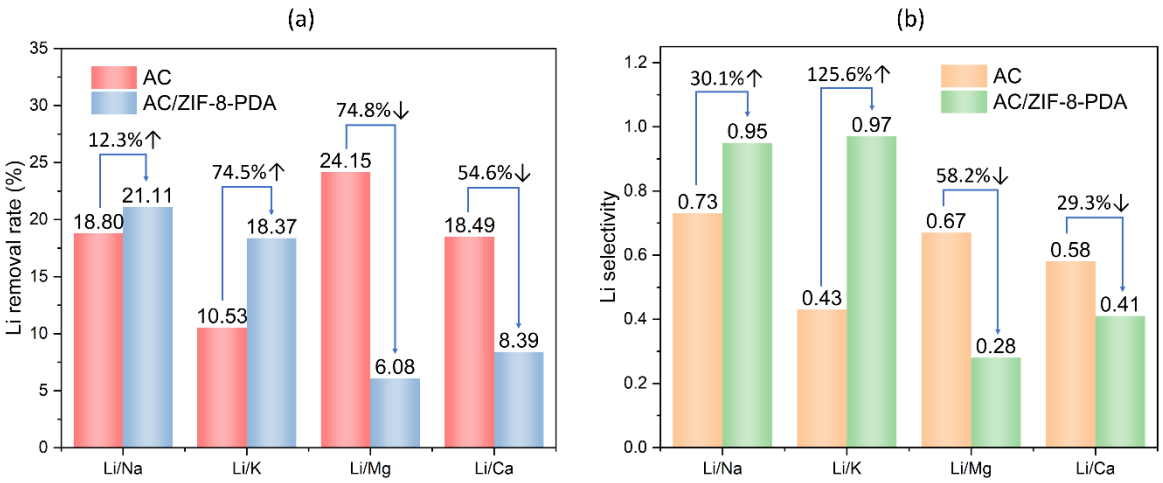

Figure 8. The changes of (a) Li removal rates and (b) Li selectivity after coating ZIF-8-PDA on AC electrodes.

3.3.2 MCDI performance under 0.5 V

The value of applied charge potential could be one of the most critical parameters influencing the MCDI performance. To investigate the Li extraction performance under different voltages, 0.5 V and 1.5 V of constant voltages were also applied for the AC/ZIF-8-PDA electrode-based MCDI system. According to the results of 1.0 V tests, a higher potential was presented to extract Li from the feed with monovalent-ion coexistence, and the electrode saturation durations were within 10 mins for both monovalent and divalent cases. Therefore, in the tests under 0.5 V and 1.5 V, samples were collected every 2 mins in the first 10 mins and every 5 mins in the last 10 mins for monovalent cases, and every 5 mins in the whole electrosorption duration for divalent cases.

The results of ion removal rates and Li extraction performance under 0.5 V are presented in **Fig. S5 and 9**. Qualitatively, Li extraction performance in monovalent cases was ascendant than in divalent cases, consistent with the results under 1.0 V. For Li/Na and Li/K binary feed, the corresponding Li removals were 13.7% and 20.5%, and Na and K removals were 9.1% and 11.0%, realizing Li selectivity of 1.50 and 1.85, respectively. For Li/Mg and Li/Ca binary feed, Li removals were 7.0% and 14.5%, while Mg and Ca removals were 12.0% and 15.7%, corresponding Li selectivity of 0.58 and 0.94, respectively. The reduced applied voltage provided weaker external stimuli for cations to span the membrane, causing the values of LAC to drop substantially. The conductivity and pH information in adsorption and desorption processes are shown in **Fig. S6**. Since fewer amounts of metal ions were adsorbed when applying the lower voltage, the final conductivity in desorption processes were also low, no higher than 300 μS/cm. On the other hand, the pH of solutions under 0.5 V remained steady since the electrodes adsorbed a small number of protons. According to the charge information shown in **Fig. S7**, CE and ENL for Na, K, Mg, and Ca coexisting feeds were estimated to be 49.3% and 10.22 μmol/L, 59.3% and 12.30 μmol/L, 22.8% and 4.73 μmol/L, and 39.5% and 8.18 μmol/L, respectively. More analysis of the influence of applied voltages is discussed in section 3.3.4.

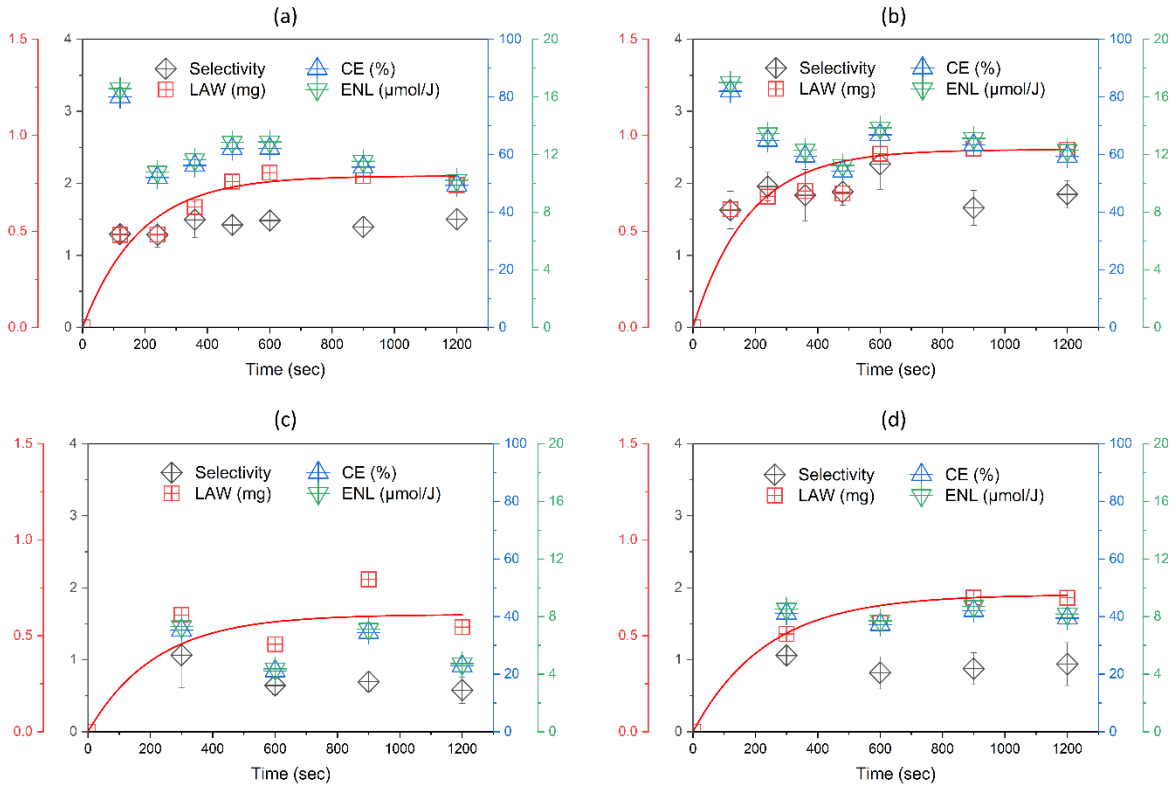

Figure 9. Temporal Li extraction performances of Li selectivity, LAW, CE, and ENL of ZIF-8-PDA coated CDI under 0.5V by using binary feed solution of (a) Li/Na, (b) Li/K, (c) Li/Mg, and (d) Li/Ca mixes.

3.3.3 MCDI performance under 1.5 V

The results of ion removal rates and Li extraction performance under 1.5 V are presented in **Fig. S8** and **10**. The removal rates of Li and the coexisting cation were approximative in monovalent cases, with 23.6% and 23.6% of Li and Na removal rates, respectively, and 24.1% and 24.1% of Li and K removal rates, respectively. Correspondingly, LAC and Li selectivity were estimated to be 2.98 mg and 1.05 in Li/Na feed and 3.01 mg and 0.95 in Li/K feed, respectively. In divalent cases, Li removal rates were distinctly lower than Mg and Ca removal rates. The ion removal rates of Li and Mg were 8.9% and 21.3%, respectively, and those of Li and Ca were 11.1% and 19.0%, respectively. Accordingly, LAC and Li selectivity in Li/Mg feed were calculated to be 1.10 mg and 0.41, slightly lower than in Li/Ca feed of 1.21 mg and 0.58, respectively. The conductivity and pH values in the adsorption and desorption processes are demonstrated in **Fig. S9**. The reduction and increase of the conductivity in ad- and desorption processes under 1.5 V were close to those under 1.0 V. The pH values rose slightly during the electrosorption process. Notably, the increase was higher in monovalent cases than in divalent cases. During desorption processes, the pH values dropped marginally in

monovalent cases yet stayed steady in divalent cases. CE and ENL were computed according to the charge data in **Fig. S10**. 35.9% and 34.1% of consumed charge were applied for Li capture in Li/Na and Li/K feeds, respectively, which were nearly double than CE in Li/Mg (14.0%) and Li/Ca (18.1%) feeds. 2.48 μmol and 2.35 μmol of Li were uptaken with every joule energy input into Li/Na and Li/K feeds, respectively, yet only 0.97 μmol and 1.25 μmol of Li were gained with per joule energy input into Li/Mg and Li/Ca feeds, respectively. More discussion about the evaluation of Li extraction performance is elaborated in section 3.3.4.

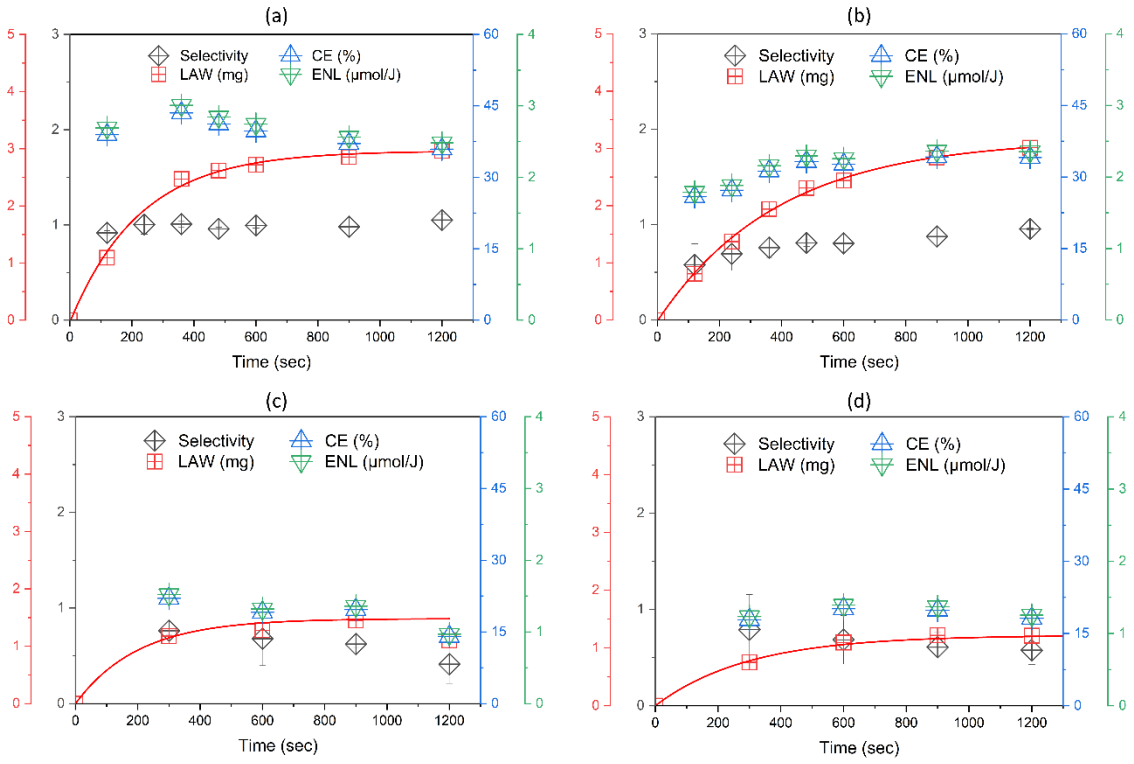

Figure 10. Temporal Li extraction performances of Li selectivity, LAW, CE, and ENL of ZIF-8-PDA coated CDI under 1.5V by using binary feed solution of (a) Li/Na, (b) Li/K, (c) Li/Mg, and (d) Li/Ca mixes.

3.3.4 Comparison of MCDI performance under different voltages

In sections 3.3.1 to 3.3.3, MCDI results under 0.5 V, 1.0 V, and 1.5 V are displayed and compared in terms of coexisting ions. In general, monovalent cases presented distinct advantages for Li capture over divalent cases under these three voltages. The Li selectivity, LAC, CE, and ENL in Li/Na feeds were over 2.5, 1.4, 2.2, and 2.2 times those in Li/Mg feeds, respectively; those in Li/K feeds were over 1.7, 1.3, 1.5, and 1.5 times those in Li/Ca feeds. Additionally, for the competing cations with the same valences, the competitiveness could depend on bare ion radius and dehydration enthalpy. The Li extraction performances in Li/K

and Li/Ca cases could be marginally superior to Li/Na and Li/Mg, respectively. The phenomena denoted that ion size, dehydration enthalpy, and valence could jointly determine ion selectivity under an electric field. In particular, the valence exhibited a more substantial influence than the ion size.

Fig. 11 concludes and compares Li extraction performances of AC/ZIF-8-PDA electrode-based MCDI under three different voltages. Overall, the metrics of Li selectivity, CE, and ENL exhibited better behaviors under lower voltages, but conversely, LAC became higher with the increase of voltages. **Fig. 11(a)** indicated a similarity of Li selectivity and a cation adsorption order of K ≈ Na ≈ Li < Ca < Mg under 1.0 V and 1.5 V. However, Li selectivity conspicuously increased to 1.4-1.9 times when the voltage lowered to 0.5 V, and the cation adsorption order switched to K < Na < Li < Ca < Mg. Notably, Li selectivity in monovalent cases exceeded 1.5 under 0.5 V, accomplishing 1.50 to Na and 1.85 to K. It might be because the cations with larger sizes need stronger driven force to squeeze into the membrane pores, but a reduced voltage could not provide enough stimuli. Under a lower voltage, fewer cations could be pushed into the membrane pores, and smaller ones were preferred. In other words, the influence of charge potentials was more significant to cations with larger sizes. The ion removal rates of larger-size cations reduced more than Li when decreasing the voltages, resulting in improved Li selectivity.

Similar to Li selectivity, as shown in **Fig. 11(b)**, the difference between LAC under 1.0 V and 1.5 V could also be neglectable. Contrary to Li selectivity, LAC under 1.0 V and 1.5 V was significantly greater than that under 0.5 V. The charge potential was the external stimuli that drove Li-ions passing through and through the membrane layer. Under low voltages, a small number of ions could effortlessly enter the nanopores due to the limited driven force; however, with the increase of voltages, a stronger driven force could push more Li-ions overcoming the restriction from the membrane. Nevertheless, the upper limit of electrode capacity and the decrease of the marginal effect would cause insufficient LAC growths with a further voltage increase from 1.0 V to 1.5 V.

For CE and ENL illustrated in **Fig. 11(c)** and **(d)**, they grew gradually with the diminution of voltages. CE and values of ENL under 0.5 V were 1.4-2.2 times and 4.1-6.5 times those under 1.5 V, respectively. It was partially because water hydrolysis occurred when the voltage was over 1.23 V and consumed more energy. In summary, applying a low voltage could achieve

higher Li selectivity, CE, and ENL, demonstrating a potential for Li extraction with low energy inputs.

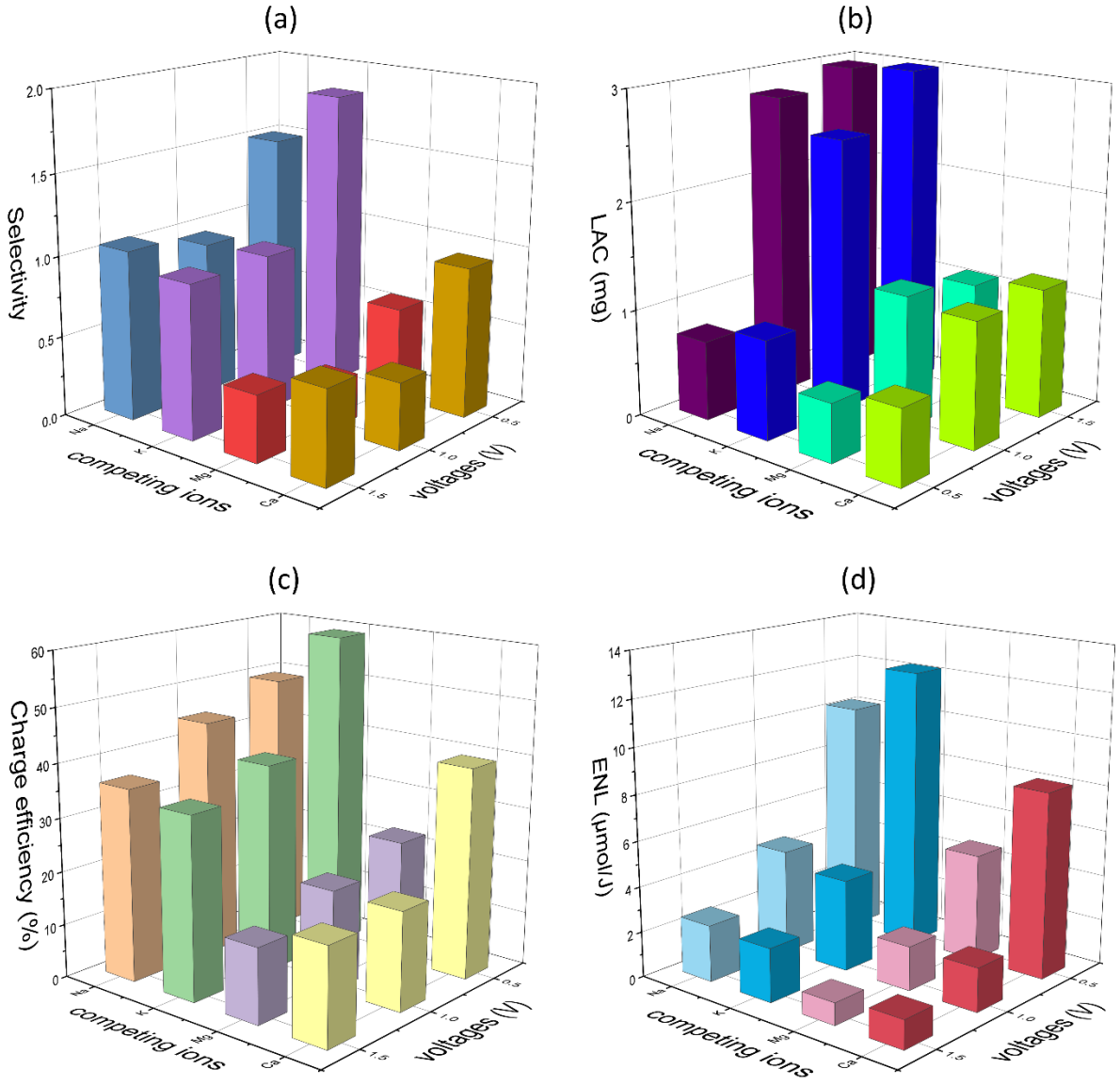

Figure 11. The comparison of Li extraction performance in binary solutions for (a) Li selectivity, (b) LAC, (c) CE, and (d) ENL of ZIF-8-PDA coated MCDI by charge potentials and competing cations.

4. Conclusions and perspectives

The rapid increase in Li demand requires effective and energy-saving techniques to extract Li from aqueous resources. In this study, AC electrodes were coated by ZIF-8-PDA membrane via the deposition coating method. ZIF-8 particles displayed great water stability with the protection of PDA. The modified electrodes were assembled in the MCDI system for Li extraction from diluted binary solutions containing Li and Na/K/Mg/Ca. The performance of

Li extraction was evaluated regarding Li selectivity, LAC, CE, and ENL. The constant voltages of 0.5 V, 1.0 V, and 1.5 V were applied to investigate the influence of charge potentials on Li extraction performances. The main findings of the electrosorption experiments are summarized as follows:

1) The presence of ZIF-8-PDA on AC electrodes enhanced Li removal rates and Li selectivity in Li/Na and Li/K binary solutions substantially but declined those in Li/Mg and Li/Ca binary solutions.
2) The performance of Li extraction in monovalent cases presented superior results than in divalent cases, which could be triggered by the sensitivity of valences to the electric field. The ion size and dehydration enthalpy could also influence Li selectivity. The MCDI system showed a slight preference for cations with smaller bare radii compared to larger ones with the same valence.
3) The applied voltages demonstrated negative relationships with Li selectivity, CE, and ENL. Li selectivity, CE, and ENL under 0.5 V were approximately 1.4-1.9, 1.4-2.1, and 4.1-6.5 times those under 1.5 V, respectively. Li selectivity in Li/Na and Li/K feeds accomplished 1.50 and 1.85 under 0.5 V, confirming the potential to selectively extract Li from seawater and SWRO brine with low energy input.
4) LAC increased greatly when the voltage raised from 0.5 V to 1.0 V, yet a higher voltage could not instigate further growth of LAC.

For clear pair comparisons of Li and its competing ions, equimolar binary solutions were used as feeds for MCDI tests in this study. However, the compositions and concentrations of cations in real-world brine are more complicated and diverse. In future work, it is necessary to investigate the performances of Li extraction using multi-component model solutions and simulated brine as feeds.

Declaration of competing interest

The authors declare that they have no known competing financial interests or personal relationships that could have appeared to influence the work reported in this paper.

Acknowledgments

This research was supported by grants from the Australian Research Council (ARC) Discovery Projects (DP230100238) and the Qatar National Research Fund under its National Priorities Research Program (NPRP 12S-0227-190166).

References

1. Yang, S., et al., *Lithium Metal Extraction from Seawater.* Joule, 2018. **2**(9): p. 1648-1651.
2. Grosjean, C., et al., *Assessment of world lithium resources and consequences of their geographic distribution on the expected development of the electric vehicle industry.* Renewable and Sustainable Energy Reviews, 2012. **16**(3): p. 1735-1744.
3. USGS, *Mineral Commodity Summaries 2022*, in *Mineral Commodity Summaries*. 2022, U.S. Geological Survey.
4. Yu, H., et al., *Metal-based adsorbents for lithium recovery from aqueous resources.* Desalination, 2022. **539**(115951).
5. Li, X., et al., *Membrane-based technologies for lithium recovery from water lithium resources: A review.* Journal of Membrane Science, 2019. **591**(117317).
6. Coterillo, R., et al., *Selective extraction of lithium from seawater desalination concentrates: Study of thermodynamic and equilibrium properties using Density Functional Theory (DFT).* Desalination, 2022. **532**(115704).
7. Orooji, Y., et al., *Recent advances in nanomaterial development for lithium ion-sieving technologies.* Desalination, 2022. **529**(115624).
8. Battistel, A., et al., *Electrochemical Methods for Lithium Recovery: A Comprehensive and Critical Review.* Adv Mater, 2020. **32**(1905440).
9. Liu, D., et al., *A closed-loop process for selective lithium recovery from brines via electrochemical and precipitation.* Desalination, 2021. **519**(115302).
10. Perez-Antolin, D., et al., *Regenerative electrochemical ion pumping cell based on semi-solid electrodes for sustainable Li recovery.* Desalination, 2022. **533**(115764).
11. Zavahir, S., et al., *A review on lithium recovery using electrochemical capturing systems.* Desalination, 2021. **500**(114883).
12. Xu, Y., et al., *High performance Mg^{2+}/Li^{+} separation membranes modified by a bis-quaternary ammonium salt.* Desalination, 2022. **526**(115519).

13. He, R., et al., *Unprecedented Mg^{2+}/Li^{+} separation using layer-by-layer based nanofiltration hollow fiber membranes.* Desalination, 2022. **525**(115492).
14. Gong, L., et al., *Direct numerical simulation of continuous lithium extraction from high Mg^{2+}/Li^{+} ratio brines using microfluidic channels with ion concentration polarization.* J Memb Sci, 2018. **556**: p. 34-41.
15. Bazrgar Bajestani, M., A. Moheb, and M. Dinari, *Preparation of lithium ion-selective cation exchange membrane for lithium recovery from sodium contaminated lithium bromide solution by electrodialysis process.* Desalination, 2020. **486**(114476).
16. Sharma, P.P., et al., *Sulfonated poly (ether ether ketone) composite cation exchange membrane for selective recovery of lithium by electrodialysis.* Desalination, 2020. **496**(114755).
17. M. Bryjak, A.S., J. Kujawski, K. Smolinska-Kempisty, W. Kujawski, *Capacitive deionization for selective extraction of lithium from aqueous solutions.* Journal of Membrane and Separation Technology, 2015. **4**: p. 110-115.
18. Sahin, S., et al., *Enhanced monovalent over divalent cation selectivity with polyelectrolyte multilayers in membrane capacitive deionization via optimization of operational conditions.* Desalination, 2022. **522**(115391).
19. Chen, Z., et al., *Ultra-durable and highly-efficient hybrid capacitive deionization by MXene confined MoS_2 heterostructure.* Desalination, 2022. **528**(115616).
20. Xing, W., et al., *Versatile applications of capacitive deionization (CDI)-based technologies.* Desalination, 2020. **482**(114390).
21. Liu, X., et al., *Cost Comparison of Capacitive Deionization and Reverse Osmosis for Brackish Water Desalination.* ACS ES&T Engineering, 2020. **1**(2): p. 261-273.
22. Choi, J., et al., *Applications of capacitive deionization: Desalination, softening, selective removal, and energy efficiency.* Desalination, 2019. **449**: p. 118-130.
23. Gamaethiralalage, J.G., et al., *Recent advances in ion selectivity with capacitive deionization.* Energy & Environmental Science, 2021. **14**(3): p. 1095-1120.
24. Chen, T.H., et al., *Cation selectivity of activated carbon and nickel hexacyanoferrate electrode materials in capacitive deionization: A comparison study.* Chemosphere, 2022. **307**(135613).
25. Suss, M.E., et al., *Water desalination via capacitive deionization: what is it and what can we expect from it?* Energy & Environmental Science, 2015. **8**(8): p. 2296-2319.
26. Porada, S., et al., *Direct prediction of the desalination performance of porous carbon electrodes for capacitive deionization.* Energy & Environmental Science, 2013. **6**(12).

27. Hu, B., et al., *Lithium ion sieve modified three-dimensional graphene electrode for selective extraction of lithium by capacitive deionization.* J Colloid Interface Sci, 2022. **612**: p. 392-400.
28. Oyarzun, D.I., et al., *Ion selectivity in capacitive deionization with functionalized electrode: Theory and experimental validation.* Water Res X, 2018. **1**(100008).
29. Shang, X., et al., *LiNi0.5Mn1.5O4-based hybrid capacitive deionization for highly selective adsorption of lithium from brine.* Separation and Purification Technology, 2021. **258**(118009).
30. Kim, B., J.Y. Seo, and C.-H. Chung, *Electrochemical Desalination and Recovery of Lithium from Saline Water upon Operation of a Capacitive Deionization Cell Combined with a Redox Flow Battery.* ACS ES&T Water, 2021. **1**(4): p. 1047-1054.
31. Shang, X., et al., *Synthesis of lithium vanadate/reduced graphene oxide with strong coupling for enhanced capacitive extraction of lithium ions.* Separation and Purification Technology, 2021. **262**(118294).
32. Jin, W., et al., *Simultaneous and precise recovery of lithium and boron from salt lake brine by capacitive deionization with oxygen vacancy-rich CoP/Co3O4-graphene aerogel.* Chemical Engineering Journal, 2021. **420**(127661).
33. Siekierka, A., *Lithium iron manganese oxide as an adsorbent for capturing lithium ions in hybrid capacitive deionization with different electrical modes.* Separation and Purification Technology, 2020. **236**(116234).
34. Ha, Y., et al., *Continuous Lithium Extraction from Aqueous Solution Using Flow-Electrode Capacitive Deionization.* Energies, 2019. **12**(15).
35. Siekierka, A., *Lithium and magnesium separation from brines by hybrid capacitive deionization.* Desalination, 2022. **527**(115569).
36. Siekierka, A. and M. Bryjak, *Selective sorbents for recovery of lithium ions by hybrid capacitive deionization.* Desalination, 2021. **520**(115324).
37. Siekierka, A., B. Tomaszewska, and M. Bryjak, *Lithium capturing from geothermal water by hybrid capacitive deionization.* Desalination, 2018. **436**: p. 8-14.
38. Xie, N., et al., *Fabricating a Flow-Through Hybrid Capacitive Deionization Cell for Selective Recovery of Lithium Ions.* ACS Applied Energy Materials, 2021. **4**(11): p. 13036-13043.
39. Choi, J., H. Lee, and S. Hong, *Capacitive deionization (CDI) integrated with monovalent cation selective membrane for producing divalent cation-rich solution.* Desalination, 2016. **400**: p. 38-46.

40. Shi, W., et al., *Efficient lithium extraction by membrane capacitive deionization incorporated with monovalent selective cation exchange membrane.* Separation and Purification Technology, 2019. **210**: p. 885-890.
41. Wang, S., et al., *Metal-Organic Framework Nanoparticles.* Adv Mater, 2018. **30**(37): p. e1800202.
42. 0. M. Yaghi, G.L., Hailian Li, *Selective binding and removal of guests in a microporous metal–organic framework.* Nature, 1995. **378**(6558): p. 703–706.
43. Liu, Y., et al., *Zeolitic imidazolate framework-based nanomaterials for the capture of heavy metal ions and radionuclides: A review.* Chemical Engineering Journal, 2021. **406**(127139).
44. Kukkar, P., et al., *Recent advances in the synthesis techniques for zeolitic imidazolate frameworks and their sensing applications.* Coordination Chemistry Reviews, 2021. **446**(214109).
45. Arafat, Y., et al., *Advances in Zeolite Imidazolate Frameworks (ZIFs) Derived Bifunctional Oxygen Electrocatalysts and Their Application in Zinc–Air Batteries.* Advanced Energy Materials, 2021. **11**(26).
46. Liu, Y., et al., *The application of Zeolitic imidazolate frameworks (ZIFs) and their derivatives based materials for photocatalytic hydrogen evolution and pollutants treatment.* Chemical Engineering Journal, 2021. **417**(127914).
47. Chin, M., et al., *Rhodamine B degradation by nanosized zeolitic imidazolate framework-8 (ZIF-8).* RSC Adv, 2018. **8**(47): p. 26987-26997.
48. Zhang, H., et al., *Ultrafast selective transport of alkali metal ions in metal organic frameworks with subnanometer pores.* Sci. Adv. , 2018. **4**(eaaq0066).
49. Mohammad, M., et al., *Metal-Phenolic network and metal-organic framework composite membrane for lithium ion extraction.* Applied Materials Today, 2020. **21**(100884).
50. Hossain, S.M., et al., *ZiF-8 induced carbon electrodes for selective lithium recovery from aqueous feed water by employing capacitive deionization system.* Desalination, 2023. **546**(116201).
51. Zheng, W. and L.Y.S. Lee, *Metal–Organic Frameworks for Electrocatalysis: Catalyst or Precatalyst?* ACS Energy Letters, 2021. **6**(8): p. 2838-2843.
52. Liu, X., et al., *Improvement of hydrothermal stability of zeolitic imidazolate frameworks.* Chem Commun (Camb), 2013. **49**(80): p. 9140-9142.

53. Zhang, H., et al., *Improving hydrostability of ZIF-8 membranes via surface ligand exchange.* Journal of Membrane Science, 2017. **532**: p. 1-8.
54. Zhang, M.-y., et al., *Improving the hydrostability of ZIF-8 membrane by biomolecule towards enhanced nanofiltration performance for dye removal.* Journal of Membrane Science, 2021. **618**(118630).
55. You, H., et al., *Advantages of polydopamine coating in the design of ZIF-8-filled thin-film nanocomposite (TFN) membranes for desalination.* Colloids and Surfaces A: Physicochemical and Engineering Aspects, 2021. **629**(127492).
56. H. Lee, S.M.D., W.M. Miller, P.B. Messersmith, *Mussel-Inspired Surface Chemistry for Multifunctional Coatings.* Science, 2007. **318**: p. 426-430.
57. Wu, X., et al., *Polydopamine tethered enzyme/metal-organic framework composites with high stability and reusability.* Nanoscale, 2015. **7**(45): p. 18883-18886.
58. Tian, Q., et al., *Polydopamine-stabilized ZIF-8: Improved water stability and lubrication performance.* Applied Surface Science, 2022. **578**(152120).
59. Sánchez-Laínez, J., et al., *Influence of ZIF-8 particle size in the performance of polybenzimidazole mixed matrix membranes for pre-combustion CO2 capture and its validation through interlaboratory test.* Journal of Membrane Science, 2016. **515**: p. 45-53.
60. Mei, X., et al., *Improving the Selectivity of ZIF-8/Polysulfone-Mixed Matrix Membranes by Polydopamine Modification for H2/CO2 Separation.* Front Chem, 2020. **8**: p. 528.
61. Zhang, H., et al., *Stability of ZIF-8 membranes and crystalline powders in water at room temperature.* Journal of Membrane Science, 2015. **485**: p. 103-111.
62. Zhang, H., M. Zhao, and Y.S. Lin, *Stability of ZIF-8 in water under ambient conditions.* Microporous and Mesoporous Materials, 2019. **279**: p. 201-210.
63. Zhang, H., et al., *Hydrolysis and condensation of ZIF-8 in water.* Microporous and Mesoporous Materials, 2019. **288**.
64. Jr., E.R.N., *Phenomenological theory of ion solvation. Effective radii of hydrated ions.* J. Phys. Chem., 1959. **63**(9): p. 1381-1387.
65. Smith, D.W., *Ionic Hydration Enthalpies.* Journal of Chemical Education, 1977. **54**(9): p. 540.
66. Seo, S.J., et al., *Investigation on removal of hardness ions by capacitive deionization (CDI) for water softening applications.* Water Res, 2010. **44**(7): p. 2267-2275.

67. Huang, D., et al., *Synergistic effects of zeolite imidazole framework@graphene oxide composites in humidified mixed matrix membranes on CO2 separation.* RSC Adv, 2018. **8**(11): p. 6099-6109.
68. Dong, L., et al., *Metal-organic framework-graphene oxide composites: A facile method to highly improve the CO2 separation performance of mixed matrix membranes.* Journal of Membrane Science, 2016. **520**: p. 801-811.
69. Yang, L., B. Tang, and P. Wu, *Metal–organic framework–graphene oxide composites: a facile method to highly improve the proton conductivity of PEMs operated under low humidity.* Journal of Materials Chemistry A, 2015. **3**(31): p. 15838-15842.
70. Hou, C.-H. and C.-Y. Huang, *A comparative study of electrosorption selectivity of ions by activated carbon electrodes in capacitive deionization.* Desalination, 2013. **314**: p. 124-129.